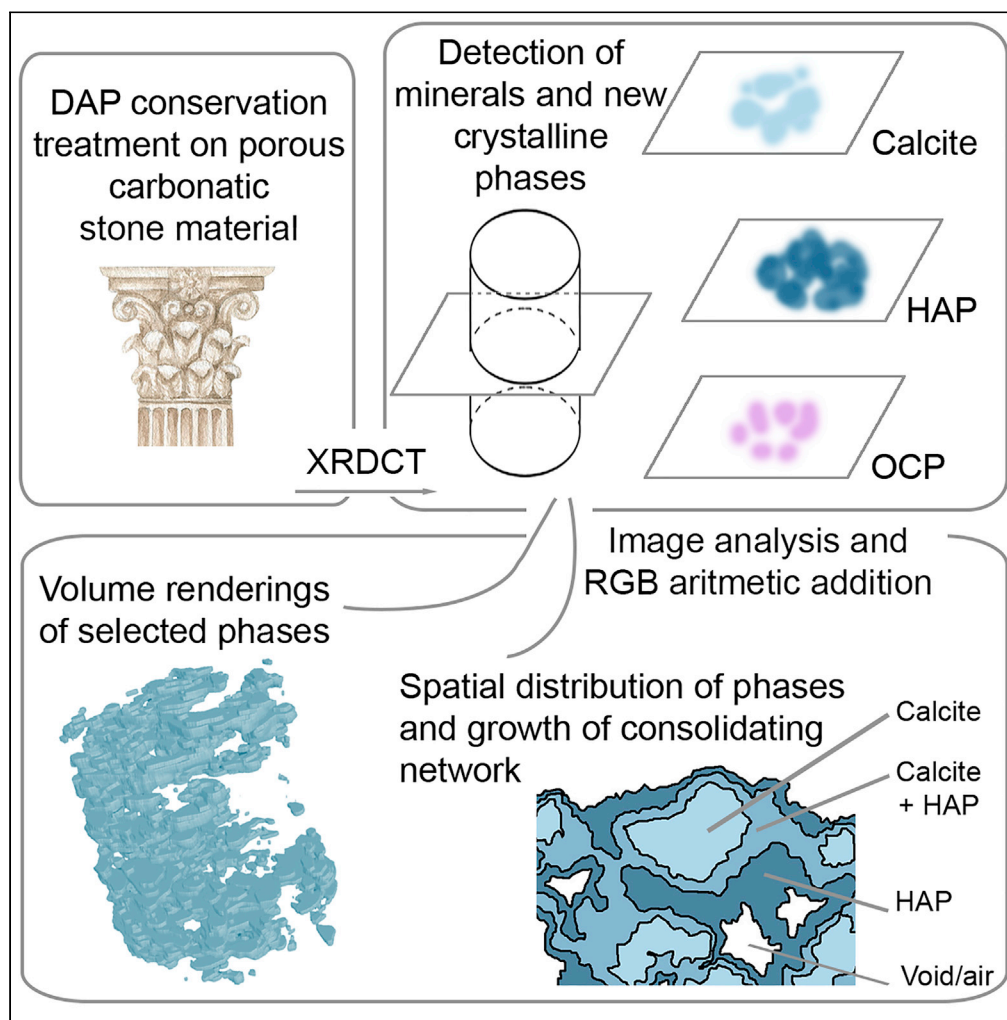CellPress
OPEN ACCESS

Article

Synchrotron X-ray diffraction computed tomography to non-destructively study inorganic treatments for stone conservation

Elena Possenti,
Claudia Conti,
Nicoletta
Marinoni, ...,
Marco Realini,
Gavin B.M.
Vaughan, Chiara
Colombo

elena.possenti@cnr.it

Highlights

DAP consolidation of a porous stone matrix is non-destructively studied by SR XRDCT

The mineralogical composition/3D distribution of phases are simultaneously explored

The 3D consolidating shell of newly formed CaPs phases is showed for the first time

XRDCT provides new analytical tools and new applications in conservation science

Article

Synchrotron X-ray diffraction computed tomography to non-destructively study inorganic treatments for stone conservation

Elena Possenti,[1,4,*] Claudia Conti,[1] G. Diego Gatta,[2] Nicoletta Marinoni,[2] Marco Merlini,[2] Marco Realini,[1] Gavin B.M. Vaughan,[3] and Chiara Colombo[1]

SUMMARY

The characterization of consolidating products formed by conservation treatments within Cultural Heritage (CH) materials is a burning issue and an analytical challenge, as non-destructive approaches, phase analysis, and volume distribution analysis are simultaneously required. This paper proposes the use of synchrotron X-ray diffraction computed tomography (XRDCT) to non-destructively study diammonium hydrogen phosphate (DAP) consolidating treatments for stone conservation. The mineralogical composition and localization of crystalline phases formed in a complex mixture have been explored and spatially resolved. The coexistence of hydroxyapatite and octacalcium phosphate has been finally demonstrated. The image analysis highlights the 3D distribution of calcium phosphates, their arrangement in a binding network down to the voxel scale, and their consolidating action. Above all, this study demonstrates the feasibility and high potential of XRDCT to investigate the interactions of conservation treatments with CH stone materials, and opens new analytical perspectives for XRDCT in conservation science and materials science.

INTRODUCTION

Synchrotron radiation (SR) X-ray diffraction micro-computed tomography (XRDCT) is a powerful technique as it provides an innovative approach in the field of material characterization by allowing the non-destructive reconstruction of the three-dimensional (3D) spatial distribution of different phases within the sample.

The technique has recently found application in diverse fields of material science, and involves the use of a micro-focused SR "pencil-beam" of X-rays to collect a set of linear projections. The scanning of the sample occurs at different angular positions during a sample rotation (in general 180° or 360°), as in a conventional micro-computed tomography (μ-CT) analysis (Kieffer et al., 2018). XRDCT collects the diffracted beam instead of the absorption/phase contrast signal (Voltolini et al., 2013) and employs tomographic inversion algorithms to reconstruct each point of the diffraction pattern. Thus, each voxel of the CT volume contains the reconstructed XRD pattern of that voxel. These data can be then used to calculate a distribution map of the phase within the sample.

Nowadays, several SR beamlines at synchrotron facilities have an experimental setup dedicated to XRDCT experiments (e.g., ID15a beamline at the European Synchrotron Radiation Facility, ESRF, Grenoble, France), and research in diverse fields is devoting increasing attention to the possible and novel applications of XRDCT. Simultaneously, more effective instrumental setups, collection algorithms, and data reduction software are being developed, see i.e. (Dong et al., 2021). XRDCT is emerging as a groundbreaking approach to overcome outstanding analytical challenges in the field of stone conservation, and overall when inorganic treatments are applied to Cultural Heritage (CH) stone materials, during their restoration. One of the main challenges concerns the need to simultaneously obtain phase maps and other spatially resolved information in multi-phase systems, after the conservation treatment; this information is not available from other routinely applied techniques. At present, absorption or phase contrast μ-CT is usually applied to extract the 3D spatial information of different phases of interest within a sample, but suffers from the difficulty in the unambiguous identification of the sample mineralogy. Moreover, X-ray diffraction and vibrational spectroscopies (i.e., Raman and FTIR) allow the identification of the mineralogical nature of

[1]Istituto di Scienze del Patrimonio Culturale (ISPC), Consiglio Nazionale delle Ricerche (CNR), Via R. Cozzi 53, 20125 Milano, Italy

[2]Dipartimento di Scienze della Terra, Università degli Studi di Milano, Via S. Botticelli 23, 20133 Milano, Italy

[3]European Synchrotron Radiation Facility, 71 Avenue des Martyrs, 38000 Grenoble, France

[4]Lead contact

*Correspondence: elena.possenti@cnr.it

https://doi.org/10.1016/j.isci.2022.105112

crystalline phases and also provide a spatially resolved dataset (either by mapping or imaging) (Bertasa et al., 2017; Cotte et al., 2022; Liu and Kazarian, 2022; Possenti et al., 2018a) but only on 2D matrices and, in many cases, invasive sample preparation is required (grinding, embedding in polished cross section, and preparation of thin sections).

On the contrary, XRDCT combines the phase sensitivity of XRD with the 3D volume resolution and mapping capability of μ–CT, providing 3D tomographic datasets and high-resolution XRD patterns at the same time, of the same volume and in a non-destructive way (Jensen et al., 2022).

Over the last years, the inorganic-mineral treatments applied to carbonatic stones are considered as an effective approach through which the stone decay is faced (Hansen et al., 2003; Matteini, 2008; Matteini et al., 2011; Sassoni et al., 2011). These treatments lead to a partial transformation of the minerals of the original matrix into newly formed phases. In particular, diammonium hydrogenphosphate (DAP, $(NH_4)_2HPO_4$) is gaining increasing attention nowadays as a reagent (Celik et al., 2020; Menningen et al., 2021; Molina et al., 2020; Murru and Fort, 2020; Sassoni et al., 2021; Sena da Fonseca et al., 2021). DAP is a water-soluble salt that reacts with the carbonatic matrix of the stone substrate and forms new calcium phosphate phases (CaPs) as a result of dissolution-recrystallization reactions occurring at the interface between the DAP solution and calcite grains (Matteini et al., 2011; Possenti et al., 2016, 2019b, 2020).

The study of DAP treatments is currently a major topic in conservation science (Defus et al., 2021a, 2021b; Possenti et al., 2019b; Sassoni, 2017, 2018), even though the comprehensive characterization of the newly formed calcium phosphates is still a challenging task and several issues on DAP treatments are still unresolved. The DAP treatments dissolve calcium ions from calcite grains, but the possible effects induced by the reagent on calcite crystals (e.g. structural variation) are still unknown (Possenti et al., 2021). Octacalcium phosphate (OCP) and hydroxyapatite (HAP) have been identified as reaction products in previous studies using a complex SR-XRD investigation (Possenti et al., 2019a). However, HAP and OCP have different stability and solubility (Dorozhkin, 2007), and their crystallization depends on the reaction conditions and the calcium ion availability (Possenti et al., 2019c, 2020, 2021; Sassoni, 2017, 2018; Wang and Nancollas, 2008). Moreover, different CaPs may be formed by DAP in different treatment modalities and/or on different stone substrates, influencing the final composition of the treated lithotypes. HAP is the most stable and insoluble phase (Dorozhkin, 2007; Wang and Nancollas, 2008).

The assessment of the actual HAP formation is a crucial step, but, at the same time, it is a challenging task for XRD (and other techniques) and in many cases the HAP formation remains uncertain, especially in presence of OCP (Drouet, 2013; Karampas and Kontoyannis, 2013). A recent study carried out by 2D XRD demonstrated that different CaPs are crystallized at different depths from the treated surface (Possenti et al., 2020), and highlights the need of 3D investigations of the consolidating phases crystal structures within stone matrices. Another important concern is the need to explore the 3D spatial distribution of CaPs with respect to calcite in the treated volume. A recent study has demonstrated the potential of 3D imaging in the characterization of the stone microstructure variation due to inorganic consolidants; in particular, μ–CT allowed the quantification of the microstructural changes in terms of porosity and pore connectivity after the DAP treatments (Possenti et al., 2019b). On the other hand, this technique fails to define the chemical nature of the newly formed crystalline phases as well as their spatial distribution in the sample volume.

In an effort to address these issues, the present research goes a step further. In particular, this study proposes and discusses the feasibility and high potential of XRDCT in the characterization of CH materials. For the first time, XRDCT is applied to map in 3D the crystallization products formed by inorganic-mineral treatments within a porous lithotype. The study is carried out on the Noto limestone, a calcarenite widely used in important Baroque buildings located in UNESCO sites in south-eastern Sicily (Italy) (Anania et al., 2012).

RESULTS AND DISCUSSION

This study compares the XRDCT investigations of untreated and DAP-treated Noto limestone with the aim of (i) assessing the variations induced by inorganic treatments to the original stone (e.g., phase composition and their 3D spatial distribution) and (ii) understanding the influence of these features on the crystallization of the new phases formed by the conservation treatment.
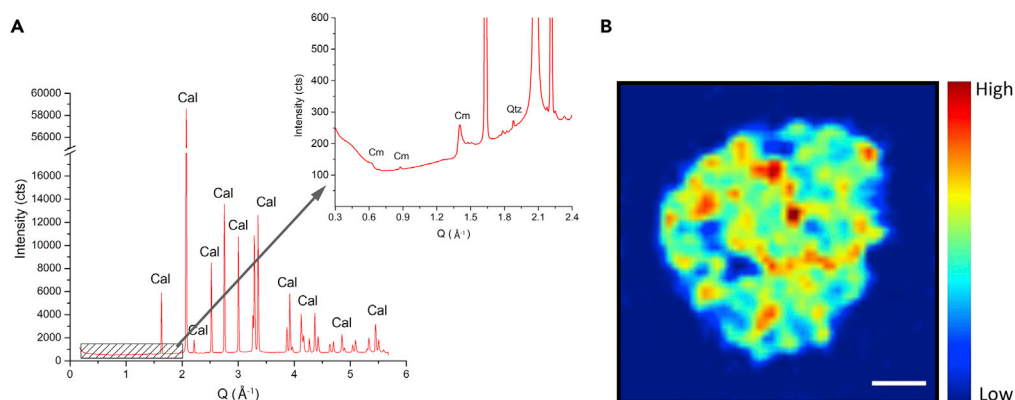
Figure 1. XRDCT investigation of the untreated Noto limestone
(A) XRD pattern extracted from a representative XRDCT slice of the untreated Noto limestone, dominated by Bragg peaks of calcite (Cal). The inset in (A) highlights the marker peaks of accessory minerals (Qtz = quartz; Cm = clay minerals).
(B) XRDCT reconstruction image showing the spatial distribution of the marker peak at Q 1.63 Å^{-1} of calcite (corresponding to the d_{012} 3.85 Å interplanar distance). Size bar: 300 μm.

To help readers to visualize the results, the data of XRDCT measurements of the untreated Noto limestone are presented as follows: the reconstructed XRD pattern of an entire representative slice is shown (Figure 1A) with peaks of the different phases identified. The spatial distribution of the phases, obtained by subtracting a local linear background and integrating the Bragg peak area in each voxel of the same slice, is displayed with false colors (Figure 1B).

The XRD pattern in Figure 1A confirms that the untreated Noto limestone is dominated by calcite with minor contents of quartz and clay minerals, which are detectable thanks to the high signal to background ratio (inset of Figure 1A). Figure 1B shows the XRDCT reconstruction image of the marker peak at Q 1.63 Å^{-1} of calcite in a representative slice, and allows the observation of the spatial distribution of calcite grains within the lithotype as well as the presence of several voids.

Figure 2 shows a comparison of the spatial distribution of calcite grains in the untreated Noto limestone by integrating the calcite peaks in the Q-ranges 1.61–1.66 Å^{-1} (max at 1.63 Å^{-1}) and 2.02–2.11 Å^{-1} (max at 2.07 Å^{-1}), corresponding to the d_{012} 3.85 Å and d_{004} 3.03 Å interplanar distances, respectively.

By comparing these two XRDCT reconstruction images, the very similar spatial distribution and relative intensity of different calcite peaks areas in the same slice suggest a random orientation of calcite crystals within Noto limestone. No artifacts due to large and single crystals are observed, meaning that the false colors in the XRDCT reconstructed images can be considered a reliable qualitative and semi-quantitative tool to investigate the spatial distribution of the crystalline phases within the bulk sample.
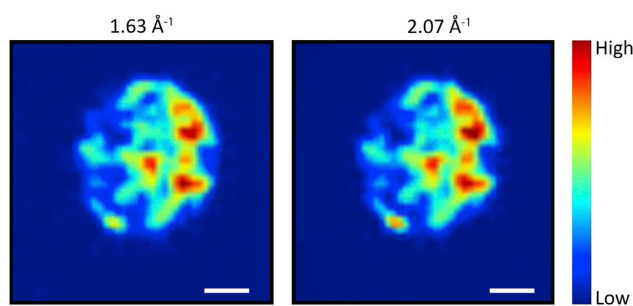

Figure 2. XRDCT reconstruction images of untreated Noto limestone
The two images shows the spatial distribution of calcite of untreated Noto limestone, obtained by integrating the peaks in the Q-range 1.61–1.66 Å^{-1} (left image, max of the XRD peak at 1.63 Å^{-1}, d_{012}) and the 2.02–2.11 Å^{-1} (right image, max of the XRD peak at 2.07 Å^{-1}, d_{004}). Size bars: 300 μm.
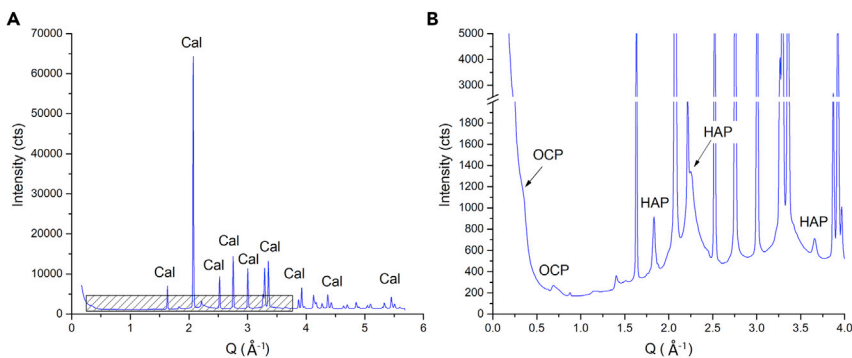
Figure 3. XRD pattern of the DAP-treated Noto limestone

(A) Full XRD pattern of the DAP-treated Noto limestone extracted by XRDCT datasets. This XRD pattern is still dominated by Bragg peaks of calcite (Cal).

(B) The detail in the 0–4 Å^{-1} Q-range of the XRD pattern shown in (A) highlights the presence of novel XRD peaks, demonstrating the crystallization of calcium phosphates (OCP, HAP) after the DAP treatment. The XRD pattern shows the presence of calcite (Cal) and of newly formed calcium phosphates (OCP, octacalcium phosphate; HAP, hydroxyapatite).

Calcite remains the predominant crystalline phase of the lithotype after the DAP treatment, as shown by the XRD pattern of Figure 3, demonstrating that the treatment does not completely transform the original minerals of the substrate into newly formed phases. Here, the significant step forward with respect to literature data is the opportunity to study the partial calcite-to-calcium phosphate conversion occurring during DAP treatments non-destructively, with microscale 3D spatial resolution.

Close inspection of the XRD pattern of Figure 3 shows clear Bragg peaks of secondary newly formed mineralogical phases, namely hydroxyapatite (HAP, $Ca(PO_4)_3(OH)$) and octacalcium phosphate (OCP, $Ca_8H_2(PO_4)_6 \cdot 5(H_2O)$). No Ca-bearing phosphates were detected in any XRD patterns or XRDCT images of untreated Noto limestone, demonstrating that HAP and OCP crystallization is the consequence of the DAP treatment. This observation supports the principal findings of this study, as the contribution of calcium phosphates from any XRD and/or tomographic image can be unambiguously attributed to newly formed reaction products and not to the biogenetic nature of the stone substrate.

A peak broadening of the main XRD reflections of OCP (0.30–0.45 Å^{-1} d_{010}, and between 0.65 and 0.75 Å^{-1}, d_{020} and d_{110}) suggests a low crystallinity phase. On the contrary, the symmetric and well-resolved diffraction peaks at Q 1.83 Å^{-1} (d_{002}), 2.24 Å^{-1} (d_{211}), and 3.66 Å^{-1} (d_{004}) prove a more ordered crystal structure for HAP.

The spatial distribution of calcite, HAP, and OCP in a representative XRDCT reconstruction image is shown Figure 4. Again, the absence of single crystal spots and/or artifacts in the XRDCT data indicates that HAP and OCP consist of tens of thousands of 3D randomly oriented crystallites, giving rise to an "ideal powder".

Calcite shows a quite complementary spatial distribution with respect to the newly formed phosphates. On the contrary, HAP and OCP share only a partial superimposition and there are volumes of interest (VOIs) where HAP and OCP appear localized alone (Figure 4, white and orange arrows, respectively). This finding is of paramount importance as it helps to answer some open questions on the nature of these two reaction products. Here, the novelty is not the detection of HAP and/or OCP, but rather their different spatial distributions, which allows the simultaneous assessment of the coexistence of these two phases in a straightforward way. HAP and OCP have been already identified by the authors by XRD after DAP treatments (Possenti et al., 2016, 2018b, 2019a). In particular, the XRD identification of OCP was quite simple, thanks to its very characteristic marker diffraction peak (d_{010}) at high interplanar distances (i.e., 18.56 Å). On the contrary, the XRD identification of HAP is more complex, especially when HAP is mixed with OCP. OCP and HAP have a similar crystalline structure, which leads to an extended overlapping of their main Bragg peaks (Drouet, 2013; Karampas and Kontoyannis, 2013). In addition, HAP generally nucleates in a poorly crystalline form, which hinders the detection of its broad peaks of much weaker intensity which are not superimposed on OCP ones. The presence of HAP on DAP-treated Carrara marble was demonstrated via an indirect method based on SR-XRD and in situ heating treatments in real time up to 900°C (Possenti et al., 2019a). Since then, the XRD identification of HAP after the DAP treatment on other lithotypes, such as
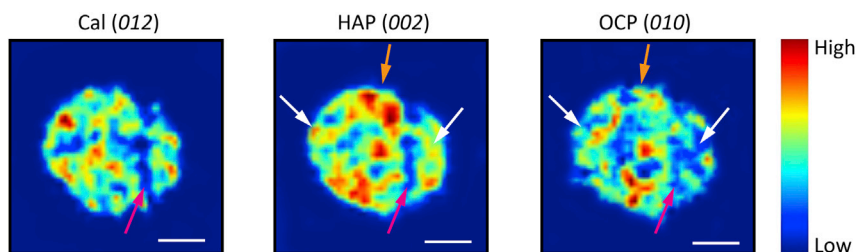
Figure 4. XRDCT reconstruction images showing the spatial distribution of calcite (Cal), hydroxyapatite (HAP), and octacalcium phosphate (OCP) within the DAP-treated Noto limestone

The XRDCT reconstruction images have been obtained by integrating the XRD marker peaks in the Q-range 1.61–1.66 Å^{-1} (max at Q 1.63 Å^{-1}, d_{012}), 1.80–1.87 Å^{-1} (max at Q 1.83 Å^{-1}, d_{002}), 0.30–0.42 Å^{-1} (max at Q ∼ 0.35 Å^{-1}, d_{010}) for Cal, HAP, and OCP, respectively. The white arrows show a region where only HAP is present; the orange arrows show regions where only OCP is formed; the purple arrows show a void of the stone substrate. Size bars: 300 μm.

Noto limestone, has been presumed (but not demonstrated) detecting the marker peaks of HAP (3.42 Å (Q 1.83 Å^{-1}) and 1.71 Å (Q 3.66 Å^{-1})) and speculating on the different intensity of XRD peaks of OCP and HAP.

In the present study, the combination of XRD data and the tomographic reconstruction images allows us to identify coexisting HAP and OCP in the same VOI, without resorting to high temperature processes and/or any sample preparation. The different shape and width of HAP and OCP Bragg peaks in the XRD patterns, as well as their different spatial distribution in the XRDCT images, finally confirms their coexistence.

The study of the spatial distribution of reaction products within the treated stone represents an enormous challenge when dealing with consolidants. One novel aspect of our study is the use of RGB color imaging for retrieving the volume distribution of a crystalline phase, which represents its semi-quantitative fraction and provides spatially resolved information.

Figure 5 shows an RGB image representing the spatial distribution of calcite and HAP within the treated Noto limestone and their split red, green, and blue channels.

The red channel highlights the regions where the HAP diffraction peak at 1.83 Å^{-1} (d_{002}) has the highest intensity and allows the visualization of the portion of the sample volume where the HAP crystallization chiefly takes place. The blue channel indicates the absence of that integrated peak, and therefore corresponds to voids within the sample, regions of air outside the sample, and/or regions occupied by other crystalline phases. Lastly, the green channel represents the volume where the integrated peak area of HAP is less intense but still present. Amazingly, the distribution map of this channel sheds light on how DAP treatments act within the stone substrates. For the first time, we can assert that the consolidants promote the growth of a crystalline network highly interconnected (here addressed at the "shell"). The shell binds the stone grains in a newly formed 3D framework and permeates the substrate. Furthermore, the arithmetic addition of images of the same color channel (red channel), but belonging to different crystalline phases, is shown in Figure 6. In the inset, the localization of calcite and HAP is shown in light blue and orange color, respectively, whereas white area refers to regions where they coexist.

Figure 6 clearly shows how HAP crystals nucleate from calcite grains of the substrate. In addition, there are regions where calcite and HAP coexist and where a 3D structure of HAP is formed within the stone. The network of HAP binds together grains of calcite and, at the same time, preserves voids within the stone material.

The volume renderings of the XRDCT datasets in Figure 7 show regions within the Noto limestone where calcite crystallites have a more compact aggregation and regions with a higher porosity. In the highly compact regions, HAP is less abundant but still present. In addition, HAP is present in the whole volume investigated by XRDCT, demonstrating the crystallization of newly formed phases down to the inner region of the stone material. It is worth highlighting that, due to viewing constraints, the volume renderings of Figure 7 are based only on the red channels of calcite and HAP, meaning that only the regions with the highest fractions of these crystalline phases are shown. However, the real binding network of calcium phosphates is
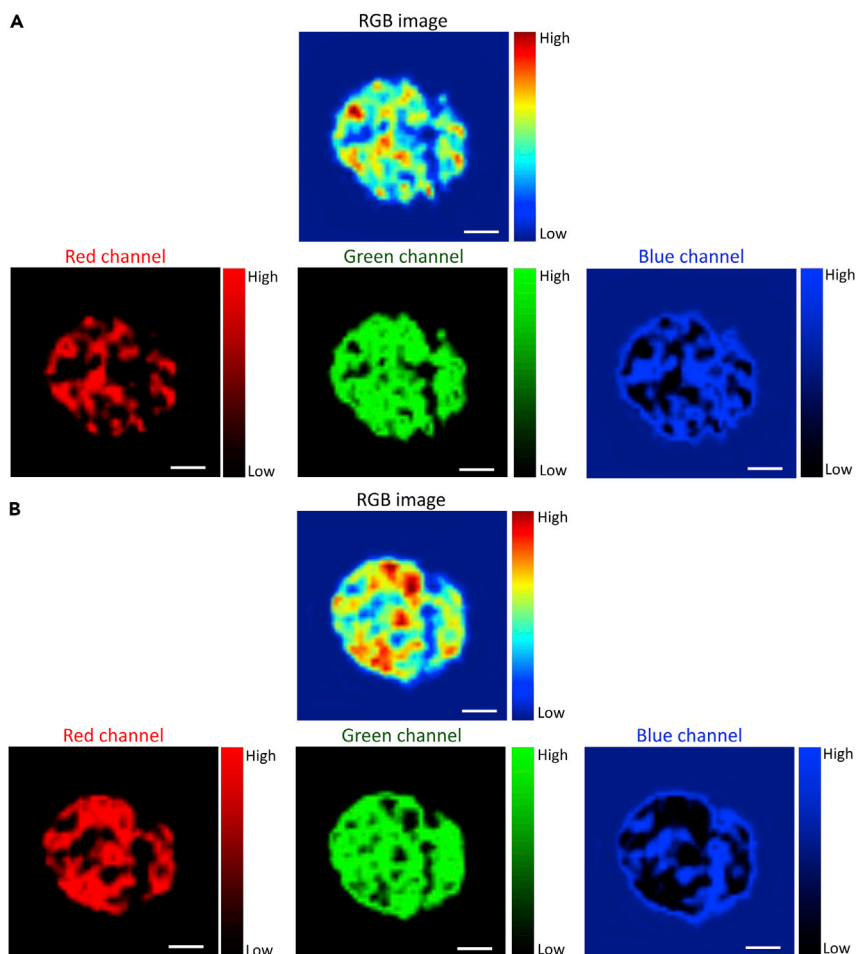
Figure 5. XRDCT image reconstruction of Cal and HAP in the DAP-treated Noto limestone

(A) RGB XRDCT image reconstruction of Cal (integrated peak in the Q-range 1.61–1.66 $\mathring{A}^{-1}$, d_{012}) and its red, green, and blue split channels. Size bars: 300 μm.

(B) RGB XRDCT image reconstruction of HAP (integrated peak in the Q-range 1.80–1.87 $\mathring{A}^{-1}$, d_{002}) and its red, green and blue split channels. Size bars: 300 μm.

unambiguously documented and it is far more interconnected and widely distributed with respect to the possibility to show it, with the volume renderings.

Limitations of the study

Limitations of the current work are mainly connected to (I) the drawbacks of the XRDCT technique itself and (II) the possible critical aspects of its feasibility in the Cultural Heritage field.

In the former case, unavoidable drawbacks are related to innate requirements of CT and XRD analyses. At first, the authors point out the need of carrying out XRDCT experiments at large-scale facilities and of identifying proper samples to be penetrable by X-rays. Therefore, the selection of the most suitable synchrotron radiation source, providing X-rays energy ranges and experimental setups *ad hoc* for specific samples, requires, in turn, an *a priori* knowledge of main hallmarks (phases) of the samples. Other *sine qua non* experimental requirements involve the need of simultaneous balancing (1) the voxel size/XRDCT spatial resolution with the sample size (samples small to achieve the highest spatial resolution but, at the same time, large (or big) enough to be representative of the investigated system), as well as (2) the X-ray energy with the range of scattering vector/interplanar distances to be investigated. Limitations exist also on the nature and features of the samples. The investigation of highly heterogeneous matrixes may result in very complex XRDCT datasets and data processing. In particular, multi-phase systems (i) composed by
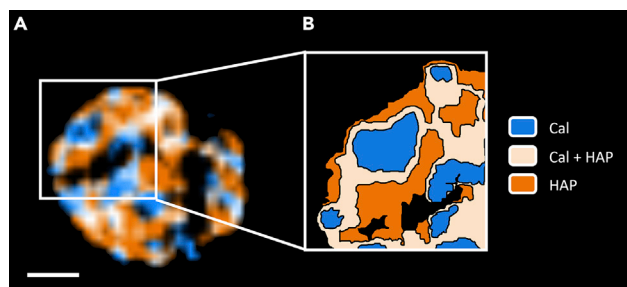
Figure 6. Spatial distribution of the red channels of calcite and of hydroxyapatite

(A) The XRDCT image reconstruction shows the spatial distribution of the red channels of calcite (Cal, in light blue) and of hydroxyapatite (HAP, in orange). The regions where calcite and hydroxyapatite coexist are shown in white/light pink. Size bar: 300 μm.

(B) Scheme of the spatial distribution of Cal, Cal + HAP, and HAP.

highly absorbing phases in mixture with low, poorly absorbing, phases, (ii) containing highly crystalline and poorly crystalline/amorphous phases, or (iii) characterized by the coexistence of several phases with diffraction signals in a wide and different angular ranges can make very complex the setup of the ideal experimental conditions for XRDCT measurements. Moreover, matrixes containing large crystallites can produce single spots superimposed on the powder diffraction rings, which, after azimuthal integration and tomographic reconstruction, may lead to line/streak artifacts in the tomograms and pose the need of developing *ad hoc* filtering approaches to deal with single-crystal artifacts.

As for the XRDCT application in conservation science, the principal limitations can be correlated with the need of a sample, which may not be always available in case the sampling of a micro-fragment from Cultural Heritage objects is not allowed. In those cases where a CH specimen is available, a further micro-sampling may be required, i.e. to achieve very high spatial resolution and high diffraction signal. Very fragile fragments and/or highly heterogeneous samples from the micro to the macro scale (i.e. with the co presence of coarse-fine grained pigments/crystals, of crystalline and amorphous phases, of inorganic and organic compounds) are very common in CH systems and this may lead to poorly representative micro-fragments, challenging experimental sessions and complex datasets. Furthermore, the X-raying of CH materials with highly brilliant SR beams can induce X-ray damages to soft/metastable/organic materials and can compromise the possibility to perform further investigations on the same sample (i.e. (Cotte et al., 2022)). Therefore, side effects and composition changes induced by X-rays should be critically evaluated prior to XRDCT measurements.

The interpretation and management of extremely large datasets might be a difficult task to overcome during the XRDCT analyses, because they usually require non-traditional instrumentations commonly used in our computer labs, such as high performance computing and/or new artificial intelligence approach.

The critical evaluation of the limitations hereby described, coupled to the development of *ad hoc* analytical protocols/sequences and *ad hoc* experimental setup, significantly contribute to fully exploit the highest potential of XRDCT in Cultural Heritage and conservation science, providing the maximum amount of high-quality information on CH materials with the minimum (or without any) damage for the investigated samples.

Progress and Potential

Advancing knowledge on the interactions occurring between conservation treatments and Cultural Heritage (CH) materials is a key point to design effective conservation strategies. In this work, we discuss the feasibility and high potential of synchrotron X-ray diffraction computed tomography (XRDCT) to non-destructively characterize the effects of conservation treatments within CH stone materials. In this study, XRDCT is applied to generate 3D maps of the crystallization products formed by inorganic-mineral treatments within a porous lithotype.
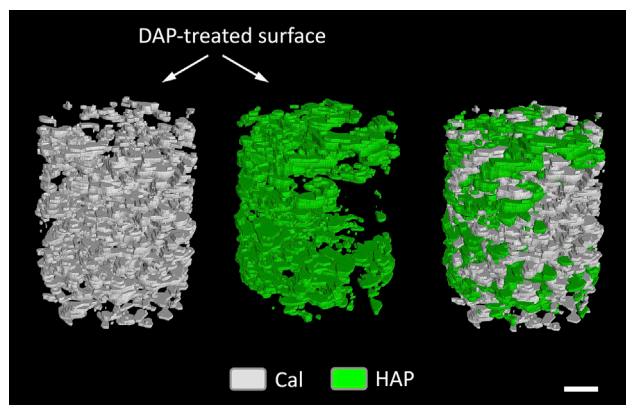
Figure 7. 3D spatial distribution of calcite and hydroxyapatite in the DAP-treated Noto limestone
Volume renderings of the DAP-treated Noto limestone showing the 3D spatial distribution of calcite in light gray (Cal; on the left) and of hydroxyapatite in green (HAP; in the middle), obtained by plotting the red channels. On the right, the spatial distributions of calcite and hydroxyapatite are superimposed to show their relative spatial localization. Size bar: 300 μm.

The strength of this approach is in its capability to (i) provide an analytical tool to support the choices of conservation yards, and to (ii) give rise to novel analytical perspectives by exploring the nature and volume distribution of original CH materials as well as novel phases formed by decay processes and other conservation treatments within heterogeneous multiphase systems.

Conclusion

This paper shows the novel application and the high potential of synchrotron radiation XRDCT to non-destructively study the nature and spatial distribution of crystalline phases formed by inorganic treatments used for stone conservation. By carrying out (i) the qualitative analysis of XRD patterns extracted from XRDCT datasets and (ii) the image analysis of XRDCT reconstruction maps and volume renderings, our study simultaneously explores the mineralogical composition and the 3D distribution of calcium phosphate phases formed by DAP consolidating treatments within the porous stone matrix of the Noto limestone.

By showing this new analytical application of XRDCT, our research overcomes a demanding analytical challenge in conservation science and answers a long-standing open question: the structural characterization and 3D localization of calcium phosphates formed by DAP treatments in a complex mixture of phases having very similar crystal structures. Here, the coexistence and spatial localization of hydroxyapatite and octacalcium phosphate have been finally demonstrated in a direct way, combining the qualitative phase analysis and image analysis, hence without resorting to high-temperature processes and/or any sample preparation. Calcite of the substrate and newly formed crystalline phases are characterized by a complementary topographic localization, with calcium phosphates nucleated on the external portion of calcite grains. Moreover, XRDCT measurements allowed the observation of the 3D crystalline network of calcium phosphates formed by the DAP treatment (the consolidating shell) that permeates the substrate down to the inner regions of the investigated VOI and, at the same time, preserves voids in the treated lithotype.

Above all, the strength of this study consists in its capability to give rise to novel analytical perspectives. By demonstrating the feasibility of XRDCT to investigate the effects induced by conservation products in CH stone materials, our study (i) provides new analytical tools to support the choices of conservation yards, and (ii) opens new analytical applications of XRDCT in conservation science, including studies focusing on the nature and volume distribution of original materials as well as novel phases formed by decay processes within heterogeneous multi-phase systems.

STAR★METHODS

Detailed methods are provided in the online version of this paper and include the following:

- KEY RESOURCES TABLE
- RESOURCE AVAILABILITY

- ○ Lead contact
- ○ Materials availability
- ○ Data and code availability
- ● METHOD DETAILS
- ○ Materials
- ○ Methods

SUPPLEMENTAL INFORMATION

Supplemental information can be found online at https://doi.org/10.1016/j.isci.2022.105112.

AUTHOR CONTRIBUTIONS

Conceptualization, E.P. and Ch.C.(Chiara Colombo); Methodology, E.P. and M.M.; Investigation, E.P., Cl.C.(Claudia Conti), N.M., and G.B.M.V.; Formal Analysis & Data Curation, E.P. and N.M.; Writing – Original Draft, E.P. and N.M.; Supervision, E.P., Ch.C., M.R., and G.D.G.

DECLARATION OF INTERESTS

The authors declare no competing interests.

INCLUSION AND DIVERSITY

We support inclusive, diverse, and equitable conduct of research.

REFERENCES

Anania, L., Badalà, A., Barone, G., Belfiore, C.M., Calabrò, C., La Russa, M.F., Mazzoleni, P., and Pezzino, A. (2012). The stones in monumental masonry buildings of the "Val di Noto" area: new data on the relationships between petrographic characters and physical–mechanical properties. Constr. Build. Mater. *33*, 122–132. https://doi.org/10.1016/j.conbuildmat.2011.12.076.

Ashiotis, G., Deschildre, A., Nawaz, Z., Wright, J.P., Karkoulis, D., Picca, F.E., and Kieffer, J. (2015). The fast azimuthal integration Python library: pyFAI. J. Appl. Crystallogr. *48*, 510–519. https://doi.org/10.1107/S1600576715004306.

Barbera, G., Barone, G., Crupi, V., Longo, F., Maisano, G., Majolino, D., Mazzoleni, P., Raneri, S., Teixeira, J., and Venuti, V. (2014). A multi-technique approach for the determination of the porous structure of building stone. Eur. J. Mineral *26*, 189–198. https://doi.org/10.1127/0935-1221/2014/0026-2355.

Bertasa, M., Possenti, E., Botteon, A., Conti, C., Sansonetti, A., Fontana, R., Striova, J., and Sali, D. (2017). Close to the diffraction limit in high resolution ATR FTIR mapping: demonstration on micrometric multi-layered art systems. Analyst *142*, 4801–4811. https://doi.org/10.1039/C7AN00873B.

Celik, S.E., Gulen, J., and Viles, H.A. (2020). Evaluating the effectiveness of DAP as a consolidant on Turkish building stones. Constr. Build. Mater. *262*, 120765. https://doi.org/10.1016/j.conbuildmat.2020.120765.

Cotte, M., Gonzalez, V., Vanmeert, F., Monico, L., Dejoie, C., Burghammer, M., Huder, L., de Nolf, W., Fisher, S., Fazlic, I., et al. (2022). The "historical materials BAG": a new facilitated access to synchrotron X-ray diffraction analyses for cultural heritage materials at the European synchrotron radiation facility. Molecules *27*, 1997. https://doi.org/10.3390/molecules27061997.

Defus, A., Possenti, E., Sansonetti, A., Tedeschi, C., Colombo, C., Biondelli, D., Vettori, S., and Realini, M. (2021a). Di-ammonium hydrogen phosphate for the consolidation of lime-based historic mortars – preliminary research. J. Cult. Herit. *48*, 45–53. https://doi.org/10.1016/j.culher.2021.01.005.

Defus, A., Sansonetti, A., Possenti, E., Tedeschi, C., Vettori, S., and Realini, M. (2021b). The effectiveness of di-ammonium hydrogen phosphate (DAP) consolidation treatment on lime-based mortars weathered by freeze-thaw cycles. J. Cult. Herit. *50*, 1–12. https://doi.org/10.1016/j.culher.2021.06.004.

Dong, H., Butler, K.T., Matras, D., Price, S.W.T., Odarchenko, Y., Khatry, R., Thompson, A., Middelkoop, V., Jacques, S.D.M., Beale, A.M., and Vamvakeros, A. (2021). A deep convolutional neural network for real-time full profile analysis of big powder diffraction data. npj Comput. Mater. *7*, 74. https://doi.org/10.1038/s41524-021-00542-4.

Dorozhkin, S.V. (2007). Calcium orthophosphates. J. Mater. Sci. *42*, 1061–1095. https://doi.org/10.1007/s10853-006-1467-8.

Drouet, C. (2013). Apatite formation: why it may not work as planned, and how to conclusively identify apatite compounds. BioMed Res. Int. *2013*, 490946. https://doi.org/10.1155/2013/490946.

Hansen, E., Doehne, E., Fidler, J., Larson, J., Martin, B., Matteini, M., Rodriguez-Navarro, C., Pardo, E.S., Price, C., de Tagle, A., et al. (2003). A review of selected inorganic consolidants and protective treatments for porous calcareous materials. Stud. Conserv. *48*, 13–25. https://doi.org/10.1179/sic.2003.48.Supplement-1.13.

Jensen, K.M., Aluri, E.R., Perez, E.S., Vaughan, G.B., Di Michel, M., Schofield, E.J., Billinge, S.J., and Cussen, S.A. (2022). Location and

characterization of heterogeneous phases within Mary Rose wood. Matter 5, 150–161. https://doi.org/10.1016/j.matt.2021.09.026.

Karampas, I.A., and Kontoyannis, C.G. (2013). Characterization of calcium phosphates mixtures. Vib. Spectrosc. 64, 126–133. https://doi.org/10.1016/j.vibspec.2012.11.003.

Kieffer, J., Petitdemange, S., and Vincent, T. (2018). Real-time diffraction computed tomography data reduction. J. Synchrotron Radiat. 25, 612–617. https://doi.org/10.1107/S1600577518000607.

La Russa, M.F., Barone, G., Belfiore, C.M., Mazzoleni, P., and Pezzino, A. (2011). Application of protective products to "Noto" calcarenite (south-eastern Sicily): a case study for the conservation of stone materials. Environ. Earth Sci. 62, 1263–1272. https://doi.org/10.1007/s12665-010-0614-3.

Liu, G.L., and Kazarian, S.G. (2022). Recent advances and applications to cultural heritage using ATR-FTIR spectroscopy and ATR-FTIR spectroscopic imaging. Analyst 147, 1777–1797. https://doi.org/10.1039/D2AN00005A.

Matteini, M. (2008). Inorganic treatments for the consolidation and protection of stone artefacts and mural paintings. Conserv. Sci. Cult. Herit. 8, 13–27. https://doi.org/10.6092/issn.1973-9494/1393.

Matteini, M., Rescic, S., Fratini, F., and Botticelli, G. (2011). Ammonium phosphates as consolidating agents for carbonatic stone materials used in architecture and cultural heritage: preliminary research. Int. J. Architect. Herit. 5, 717–736. https://doi.org/10.1080/15583058.2010.495445.

Menningen, J., Sassoni, E., Sobott, R., and Siegesmund, S. (2021). Constraints of the durability of inorganic and organic consolidants for marble. Environ. Earth Sci. 80, 370. https://doi.org/10.1007/s12665-021-09664-w.

Molina, E., Arizzi, A., Benavente, D., and Cultrone, G. (2020). Influence of surface finishes and a calcium phosphate-based consolidant on the decay of sedimentary building stones due to acid attack. Front. Mater. 7, 1–18. https://doi.org/10.3389/fmats.2020.581979.

Murru, A., and Fort, R. (2020). Diammonium hydrogen phosphate (DAP) as a consolidant in carbonate stones: impact of application methods on effectiveness. J. Cult. Herit. 42, 45–55. https://doi.org/10.1016/j.culher.2019.09.003.

Possenti, E., Colombo, C., Bersani, D., Bertasa, M., Botteon, A., Conti, C., Lottici, P.P., and Realini, M. (2016). New insight on the interaction of diammonium hydrogenphosphate conservation treatment with carbonatic substrates: a multi-analytical approach. Microchem. J. 127, 79–86. https://doi.org/10.1016/j.microc.2016.02.008.

Possenti, E., Colombo, C., Conti, C., Gigli, L., Merlini, M., Plaisier, J.R., Realini, M., and Gatta, G.D. (2018a). What's underneath? A non-destructive depth profile of painted stratigraphies by synchrotron grazing incidence X-ray diffraction. Analyst 143, 4290–4297. https://doi.org/10.1039/C8AN00901E.

Possenti, E., Colombo, C., Conti, C., Gigli, L., Merlini, M., Plaisier, J.R., Realini, M., and Gatta, G.D. (2018b). Grazing incidence synchrotron X-ray diffraction of marbles consolidated with diammonium hydrogen phosphate treatments: non-destructive probing of buried minerals. Appl. Phys. A 124, 383. https://doi.org/10.1007/s00339-018-1798-8.

Possenti, E., Colombo, C., Conti, C., Gigli, L., Merlini, M., Plaisier, J.R., Realini, M., Sali, D., and Gatta, G.D. (2019a). Diammonium hydrogenphosphate for the consolidation of building materials. Investigation of newly-formed calcium phosphates. Constr. Build. Mater. 195, 557–563. https://doi.org/10.1016/j.conbuildmat.2018.11.077.

Possenti, E., Colombo, C., Conti, C., Marinoni, N., Merlini, M., Negrotti, R., Realini, M., and Gatta, G.D. (2019b). Consolidation of building materials with a phosphate-based treatment: effects on the microstructure and on the 3D pore network. Mater. Charact. 154, 315–324. https://doi.org/10.1016/j.matchar.2019.05.037.

Possenti, E., Colombo, C., Realini, M., Song, C.L., and Kazarian, S.G. (2021). Time-resolved ATR–FTIR spectroscopy and macro ATR–FTIR spectroscopic imaging of inorganic treatments for stone conservation. Anal. Chem. 93, 14635–14642. https://doi.org/10.1021/acs.analchem.1c02392.

Possenti, E., Conti, C., Gatta, G.D., Merlini, M., Realini, M., and Colombo, C. (2020). Synchrotron radiation µ X-ray diffraction in transmission geometry for investigating the penetration depth of conservation treatments on cultural heritage stone materials. Anal. Methods 12, 1587–1594. https://doi.org/10.1039/D0AY00010H.

Possenti, E., Conti, C., Gatta, G.D., Realini, M., and Colombo, C. (2019c). Diammonium hydrogenphosphate treatment on dolostone: the role of Mg in the crystallization process. Coatings 9, 169. https://doi.org/10.3390/coatings9030169.

Sassoni, E. (2018). Hydroxyapatite and other calcium phosphates for the conservation of cultural heritage: a review. Materials 11, 557. https://doi.org/10.3390/ma11040557.

Sassoni, E. (2017). Phosphate-based treatments for conservation of stone. RILEM Tech. Lett. 2, 14–19. https://doi.org/10.21809/rilemtechlett.2017.34.

Sassoni, E., Delhomme, C., Forst, S., Graziani, G., Hénin, J., Masi, G., Palazzo, A., Rolland, O., and Vergès-Belmin, V. (2021). Phosphate treatments for stone conservation: 3-year field study in the Royal Palace of Versailles (France). Mater. Struct. 54, 140. https://doi.org/10.1617/s11527-021-01717-7.

Sassoni, E., Naidu, S., and Scherer, G.W. (2011). The use of hydroxyapatite as a new inorganic consolidant for damaged carbonate stones. J. Cult. Herit. 12, 346–355. https://doi.org/10.1016/j.culher.2011.02.005.

Schindelin, J., Arganda-Carreras, I., Frise, E., Kaynig, V., Longair, M., Pietzsch, T., Preibisch, S., Rueden, C., Saalfeld, S., Schmid, B., et al. (2012). Fiji: an open-source platform for biological-image analysis. Nat. Methods 9, 676–682. https://doi.org/10.1038/nmeth.2019.

Sena da Fonseca, B., Ferreira Pinto, A.P., Piçarra, S., Caldeira, B., and Montemor, M.F. (2021). Consolidating efficacy of diammonium hydrogen phosphate on artificially aged and naturally weathered coarse-grained marble. J. Cult. Herit. 51, 145–156. https://doi.org/10.1016/j.culher.2021.08.003.

Vamvakeros, A., Jacques, S.D.M., Di Michiel, M., Senecal, P., Middelkoop, V., Cernik, R.J., and Beale, A.M. (2016). Interlaced X-ray diffraction computed tomography. J. Appl. Crystallogr. 49, 485–496. https://doi.org/10.1107/S160057671600131X.

Vaughan, G.B.M., Baker, R., Barret, R., Bonnefoy, J., Buslaps, T., Checchia, S., Duran, D., Fihman, F., Got, P., Kieffer, J., et al. (2020). ID15A at the ESRF - a beamline for high speed operando X-ray diffraction, diffraction tomography and total scattering. J. Synchrotron Radiat. 27, 515–528. https://doi.org/10.1107/S1600577519016813.

Voltolini, M., Dalconi, M.C., Artioli, G., Parisatto, M., Valentini, L., Russo, V., Bonnin, A., and Tucoulou, R. (2013). Understanding cement hydration at the microscale: new opportunities from 'pencil-beam' synchrotron X-ray diffraction tomography. J. Appl. Crystallogr. 46, 142–152. https://doi.org/10.1107/S0021889812046985.

Wang, L., and Nancollas, G.H. (2008). Calcium orthophosphates: crystallization and dissolution. Chem. Rev. 108, 4628–4669. https://doi.org/10.1021/cr0782574.

STAR★METHODS

KEY RESOURCES TABLE

REAGENT or RESOURCE	SOURCE	IDENTIFIER
Chemicals, peptides, and recombinant proteins		
Diammonium hydrogen phosphate	Sigma-Aldrich	CAS Number 7783–28-0
Cellulose pulp	Phase	MH 300
Deposited data		
Analyzed data	This paper	https://doi.org/10.1016/j.isci.2022.105112
Software and algorithms		
Locally modified version of PyFAI	https://doi.org/10.1107/S1600576715004306; https://doi.org/10.1107/S1600577518000607	N/A
X'Pert HighScore 2.2.0	PANalytical	https://panalytical-x-pert-highscore.software.informer.com/2.2/
Fiji	ImageJ	https://imagej.net/software/fiji/downloads
VGStudio 2.0	Volume Graphics	https://www.volumegraphics.com/en/products/vgstudio.html

RESOURCE AVAILABILITY

Lead contact

Further information and requests for resources, reagents and datasets should be directed to and will be fulfilled by the lead contact, Elena Possenti (elena.possenti@cnr.it).

Materials availability

This study did not generate new unique reagents.

Data and code availability

- The data reported in this paper will be shared by the Lead contact upon request.

- This paper does not report original code.

- Any additional information required to reanalyze the data reported in this paper is available from the Lead contact upon request.

METHOD DETAILS

Materials

The investigations were carried out on the Noto yellowish limestone, a porous biomicrite outcropping in the Val di Noto (south-eastern Sicily). This variety is mainly composed of calcite; the microstructure is irregular, and displays an allochemical content of about 30%, mainly consisting of bioclasts and peloids. The matrix is mainly micritic and microsparitic, while sparry cement occurs only within foraminifera (Anania et al., 2012; Barbera et al., 2014; La Russa et al., 2011). This particular calcarenite has been selected as a reference system to investigate the interactions of DAP treatments (3D diffusion and crystallisation of new CaPs phases) with highly porous stone matrices having micritic calcite (see i.e. La Russa et al., 2011; Possenti et al., 2020, 2019b, 2016). The XRDCT measurements were performed on an untreated lithotype and on a lithotype treated with DAP. The DAP treatments were carried out by poultice on a set of freshly quarried prismatic specimens (50 × 50 × 20 mm) with a 0.76 M DAP water solution (DAP CAS Number 7783–28-0, assay ≥99.0%, reagent grade; dry cellulose pulp MH 300 Phase, Italy; poultice ratio ∼5:1 DAP solution: cellulose pulp). A poultice layer of ∼1–1.5 cm was applied on the specimen surface and a sheet of Japanese paper was placed between the paper poultice and the stone surface, to prevent damages due to the sticking of the poultice after drying. The treatment time was 2 h and during the consolidating

treatment the specimens were wrapped in a plastic film to avoid the evaporation of the solution (Possenti et al., 2019b). At the end of the treatment, the plastic film was removed and the specimens were left drying at room temperature for 24 h with the poultice on top. After that, the poultice was then removed and all the specimens were rinsed three times by immersion in Milli-Q water to remove the possible soluble phases (unreacted DAP and reaction byproducts) and dried again. Suitable fragments for XRDCT (cylinders with diameter 1.5–1.0 mm) were sampled from untreated and treated 50 × 50 × 20 mm specimens. Figure S1 shows the XRDCT experimental setup of Noto limestone stone samples mounted in the ID15a beamline.

Methods

The XRDCT investigations were carried out at the ID15a beamline (Vaughan et al., 2020) of the ESRF (European Synchrotron Radiation facility; Grenoble, France) during the beamtime allocated for the proposal nr. 80828. The cylindrical samples were mounted on a sample stage which allowed translational and rotational movements. The energy of the monochromatic beam was tuned to 42 keV using a double-bounce bent Laue monochromator, and focused down to the micrometre scale (35 µm (h)×15 µm (v)) using a compound refractive lens transfocator.

The XRDCT scans along y were collected over a 180° rotation (ω) (Vamvakeros et al., 2016). The slice thickness was equal to the vertical beam size (15 µm). The total measuring time for each XRDCT dataset was ~8 h.

A Pilatus 3 × 2M CdTe area detector was used to collect the diffractograms. Detector distance and other geometric parameters were calibrated from diffractograms of a capillary sample of NIST SRM674b CeO_2 using PyFAI, a locally modified version of which (Ashiotis et al., 2015; Kieffer et al., 2018) was also used to azimuthally integrate the projections with outlier rejection to minimize a skewing effect due to the possible presence of large crystallites. Projections were rearranged into sinograms which were subsequently centered and corrected for background scattering. Beamline scripts were then used to perform and interpret tomographic reconstructions of the integrated data. With this experimental setup, the field of view (FOV) was 1.8 ×1.8 ×1.5 mm and the reconstructed images (tomograms) have a final voxel size of 35 ×35 ×15 µm. The samples were aligned within the FOV in order to focus either the treated surface or the inner regions.

The XRDCT reconstruction images of selected crystalline phases were extracted from the XRDCT datasets by plotting the integrated area of the marker XRD peaks as a function of all pixels of the array. The XRDCT reconstruction images, representing the 3D spatial distribution of specific XRD peaks, are presented in a false color colourmap spanning from red to green-blue hues and corresponding to regions having a high or low integrated area, respectively. The size of each slice, and thus of each XRDCT reconstruction image, obtained with this setup is 1800 × 1800 × 15 µm. The XRDCT reconstruction images and the XRD patterns were obtained from the XRDCT tomographic datasets by using the software/python scripts available at the ID15a beamline.

The XRD patterns were extracted from individual voxels or whole slices of the 3D mineralogical maps. The XRD patterns were not subjected to any smoothing or post-processing. The qualitative analysis of the XRD patterns was carried out with the X'Pert HighScore 2.2.0 software and database (PANalytical). The XRDCT reconstructed slices have been visualized using the open source Fiji software (Schindelin et al., 2012), while 3D image renderings have been obtained with the commercial software VGStudio 2.0 (Volume Graphics, Germany).